of wave-vectors. The calibration reference was again an area of bare Si adjacent to the 3D PhC device. Spatially localized reflection measurements were performed by placing the lensed fibre at normal-incidence in a confocal geometry. The reflected light was collected and measured with the same fibre (Fig. 4b, inset).

Numerical simulation

We used the FDTD method to solve the full-vector time-dependent Maxwell's equations on a computational grid. This method is exact up to the discretization error (which in our case is about 1–2%). The only input used was the sample's feature sizes. The lateral size of the computational cell consists of a 16 × 8 arrangement of the minimum orthogonal unit cell and corresponds to a 9 μm × 7.8 μm area. In the vertical direction, the cell consists of the seven PhC layers on top of a semi-infinite substrate. For amorphous Si in the range of 1.1 μm to 1.6 μm we used an average dielectric constant of 12. Defects were introduced in the second layer (see Fig. 1b) in a non-periodic distribution at a density of about 15%. Bloch-periodic boundary conditions were applied laterally and absorbing (perfectly matched layers) boundary regions vertically. A laterally plane and temporally gaussian source was introduced at the top of the computational cell, and fields and fluxes monitored both above and below the PhC. Upon Fourier transforming the fields and fluxes, we obtain the frequency-resolved reflectance and transmittance.

Received 20 December 2003; accepted 19 April 2004; doi:10.1038/nature02575.

1. Yablonovitch, E. Inhibited spontaneous emission in solid-state physics and electronics. *Phys. Rev. Lett.* **58,** 2059–2062 (1987).
2. John, S. Strong localization of photons in certain disordered dielectric superlattices. *Phys. Rev. Lett.* **58,** 2486–2489 (1987).
3. Joannopoulos, J. D., Meade, R. D. & Winn, J. N. *Photonic Crystals* (Princeton Press, Princeton, New Jersey, 1995).
4. Joannopoulos, J. D., Villeneuve, P. R. & Fan, S. Photonic crystals: putting a new twist on light. *Nature* **386,** 143–149 (1997).
5. Fleming, J. G. & Lin, S. Y. Three-dimensional photonic crystal with a stop band from 1.35 to 1.95 μm. *Opt. Lett.* **24,** 49–51 (1999).
6. Noda, S., Tomoda, K., Yamamoto, N. & Chutinan, A. Full three-dimensional photonic bandgap crystals at near-infrared wavelengths. *Science* **289,** 604–606 (2000).
7. Campbell, M., Sharp, D. N., Harrison, M. T., Denning, R. G. & Turberfield, A. J. Fabrication of photonic crystals for the visible spectrum by holographic lithography. *Nature* **404,** 53–56 (2000).
8. Vlasov, Y. A., Bo, X. Z., Sturm, J. C. & Norris, D. J. On-chip natural assembly of silicon photonic bandgap crystals. *Nature* **414,** 289–293 (2001).
9. Blanco, A. *et al.* Large-scale synthesis of a silicon photonic crystal with a complete three-dimensional bandgap near 1.5 micrometres. *Nature* **405,** 437–440 (2000).
10. Cheng, C. C. & Scherer, A. Fabrication of photonic band-gap crystals. *J. Vac. Sci. Technol. B* **13,** 2696–2700 (1995).
11. Aoki, K. *et al.* Three-dimensional photonic crystals for optical wavelengths assembled by micromanipulation. *Appl. Phys. Lett.* **81,** 3122–3124 (2002).
12. Kennedy, S. R., Brett, M. J., Toader, O. & John, S. Fabrication of tetragonal square spiral photonic crystals. *Nano Lett.* **2,** 59–62 (2002).
13. Kuramochi, E. *et al.* A new fabrication technique for photonic crystals: nanolithography combined with alternating-layer deposition. *Opt. Quant. Elec.* **34,** 53–61 (2002).
14. Sato, T. *et al.* Photonic crystals for the visible range fabricated by autocloning technique and their application. *Opt. Quant. Elec.* **34,** 63–70 (2002).
15. Johnson, S. G. & Joannopoulos, J. D. Three-dimensional periodic dielectric layered structure with omnidirectional photonic band gap. *Appl. Phys. Lett.* **77,** 3490–3492 (2000).
16. Povinelli, M. L., Johnson, S. G., Fan, S. & Joannopoulos, J. D. Emulation of two-dimensional photonic crystal defect modes in a photonic crystal with a three-dimensional photonic band gap. *Phys. Rev. B* **64,** 075313 (2001).
17. Lidorikis, E., Povinelli, M. L., Johnson, S. G. & Joannopoulos, J. D. Polarization-independent linear waveguides in 3D photonic crystals. *Phys. Rev. Lett.* **91,** 023902 (2003).
18. Johnson, S. G. & Joannopoulos, J. D. Block-iterative frequency-domain methods for Maxwell's equations in a planewave basis. *Opt. Express* **8,** 173–190 (2001).
19. Kunz, K. S. & Luebbers, R. J. *The Finite-Difference Time-Domain Methods* (CRC, Boca Raton, Florida, 1993).
20. Sting, D. W. & Messerschmidt, R. G. Reflective beam splitting objective. US patent 4,653,880 (1987).
21. Nicholson, J. W. *et al.* All-fiber, octave-spanning supercontinuum. *Opt. Lett.* **28,** 643–645 (2003).
22. Savas, T. A., Schattenburg, M. L., Carter, J. M. & Smith, H. I. Large-area achromatic interferometric lithography for 100 nm period gratings and grids. *J. Vac. Sci. Technol. B* **14,** 4167–4170 (1996).
23. Qi, M. & Smith, H. I. Achieving nanometer-scale, controllable pattern shifts in x-ray lithography using an assembly-tilting technique. *J. Vac. Sci. Technol. B* **20,** 2991–2994 (2002).
24. Chou, S. Y., Krauss, P. R. & Renstrom, P. J. Imprint lithography with 25-nanometer resolution. *Science* **272,** 85–87 (1996).
25. Boegli, V. & Kern, D. P. Automatic mark detection in electron beam nanolithography using digital image processing and correlation. *J. Vac. Sci. Technol. B* **8,** 1994–2001 (1990).

Supplementary Information accompanies the paper on **www.nature.com/nature**.

Acknowledgements We would like to thank M. Mondol and J. Daley for experimental assistance, and M. Povinelli for helpful discussions. The work was supported in part by a grant from the Materials Research Science and Engineering Center program of the National Science Foundation.

Competing interests statement The authors declare that they have no competing financial interests.

Correspondence and requests for materials should be addressed to M.Q. (mqi@alum.mit.edu).

Release of methane from a volcanic basin as a mechanism for initial Eocene global warming

Henrik Svensen[1], Sverre Planke[1,2], Anders Malthe-Sørenssen[1], Bjørn Jamtveit[1], Reidun Myklebust[3], Torfinn Rasmussen Eidem[2] & Sebastian S. Rey[2]

[1]*Physics of Geological Processes, University of Oslo, PO Box 1048 Blindern, 0316 Oslo, Norway*
[2]*Volcanic Basin Petroleum Research (VBPR), Oslo Research Park, 0349 Oslo, Norway*
[3]*TGS-NOPEC Geophysical Company, 3478 Nærsnes, Norway*

A 200,000-yr interval of extreme global warming marked the start of the Eocene epoch about 55 million years ago. Negative carbon- and oxygen-isotope excursions in marine and terrestrial sediments show that this event was linked to a massive and rapid (~10,000 yr) input of isotopically depleted carbon[1,2]. It has been suggested previously that extensive melting of gas hydrates buried in marine sediments may represent the carbon source[3,4] and has caused the global climate change. Large-scale hydrate melting, however, requires a hitherto unknown triggering mechanism. Here we present evidence for the presence of thousands of hydrothermal vent complexes identified on seismic reflection profiles from the Vøring and Møre basins in the Norwegian Sea. We propose that intrusion of voluminous mantle-derived melts in carbon-rich sedimentary strata in the northeast Atlantic may have caused an explosive release of methane—transported to the ocean or atmosphere through the vent complexes—close to the Palaeocene/Eocene boundary. Similar volcanic and metamorphic processes may explain climate events associated with other large igneous provinces such as the Siberian Traps (~250 million years ago) and the Karoo Igneous Province (~183 million years ago).

A huge magmatic complex of dominantly subhorizontal sheets (sills) of basaltic composition intruded the Cretaceous Vøring and Møre basins before, and during, the northeast Atlantic continental break-up about 55 million years (Myr) ago[5–7]. The sill complex covers an area of at least 80,000 km^2 (Fig. 1), but sills are also likely to be present in basin segments covered by lava flows that inhibit deep imaging (for example, beneath the 13,000 km^2 large 'Inner Flows' region). The thickness and number of sills is difficult to map as subsill seismic imaging is often poor. However, both field and seismic data commonly reveal several levels of sill intrusions[6,8,9]. Three sills were drilled by the well 6607/5-2 with thicknesses of 2, 91 and >50 m (refs 6, 10). The middle sill is very well imaged on seismic reflection data, and can be followed for >50 km into the Vøring Basin. A conservative estimate of the volume of the sill complex in the Vøring and Møre basins is 0.9–2.5 × 10^4 km^3 on the basis of an intruded area of 85,000 km^2 and an average vertical accumulated sill thickness of 100–300 m. The area of the entire sill complex in the North Atlantic Volcanic Province (NAVP) is probably at least five times greater than the sill complex in the Vøring and Møre basins. This estimate is based on the fact that the two studied basins comprise only 10% of the length of the northeast Atlantic volcanic margins, and a conservative estimate of the width of the NAVP sill complex being 50% of the width of the Vøring and Møre basins sill complex.

We have identified and characterized 735 hydrothermal vent complexes in the Vøring and Møre basins (Figs 1, 2 and 3). The total number of complexes in the Møre and Vøring basins is estimated to be at least 3–5 times greater, given the size distribution of the vent complexes and the seismic line coverage. This factor has

been confirmed by comparing the number of vent complexes identified on two- and three-dimensional (2D and 3D) seismic data in the same region. The hydrothermal vent complexes represent pipe-like structures with upper parts consisting of craters or mounds[11–13]. Geochemical and petrographic data from the Vøring Basin and the Karoo Basin in South Africa show that vent complexes are affected by hydrothermal fluids (ref. 14 and Methods). Hydrothermal vent complexes are interpreted to originate in contact aureoles around sill intrusions, and formed by explosive release of fluids and sediments shortly (tens of years) after sill emplacement[11–13].

Constraints on the timing of magma emplacement, and thus vent complex formation, can be obtained from seismic interpretation and biostratigraphy. The seismic interpretation reveals that the intrusive volcanism occurred mainly before the main extrusive events because: (1) the Top Palaeocene horizon (the stratigraphic level where >95% of the hydrothermal vent complexes terminate) continues beneath the extrusive Inner Flows; and (2) no hydrothermal vent complexes have been identified within or above the extrusive sequence (Fig. 1). Careful interpretation shows that most vent complexes terminate at the same stratigraphic level, the Top Palaeocene, except for 20 vent complexes in the Møre Basin that terminate within the Palaeocene sequence.

New biostratigraphic dating of the hydrothermal vent complex drilled by 6607/12-1 (Fig. 3) shows that this vent complex was formed during the TP5a palynozone (55.0 to 55.8 Myr ago[15]), most probably at the start of the initial Eocene thermal maximum (IETM). This interpretation is based on the presence of abundant immature *Apectodinium augustum* palynomorphs in a 25-m interval above the lower contact of the 'eye' structure and a few *in situ* mature *A. augustum* palynomorphs just below this interface. The increase of *A. augustum* is consistent with a worldwide increase of *A. augustum* during the IETM[16], whereas the mature palynomorphs suggest a local heating event related to the formation of the hydrothermal vent complex that occurred just before the *A. augustum* bloom. Note that our timing is consistent with the timing of sill emplacement in the Faeroe–Shetland Basin obtained from seismic interpretation and biostratigraphic dating[17].

Both field and seismic data suggest that the major part of the sill complexes were formed in a short time span. Individual sills in the NAVP may be up to hundreds of kilometres long and must have formed very rapidly (tens of years) to avoid solidification. Seismic observations indicate that a small number of large-volume intrusive episodes have formed the entire intrusive complex of the Vøring and Møre basins. For comparison, single flows with volumes exceeding 2,000 km^3 have been estimated in the Columbia River Flood Basalt Province[18] (that is, 4 to 12 such events may form the entire Vøring and Møre basins sill complex), but even larger individual events can be expected in the much more voluminous NAVP.

Our hypothesis of a rapid melt emplacement is further corroborated by volcanological arguments. The flux of melts into sedimentary basins is ultimately controlled by the rate of melt extraction from the mantle source. A conservative estimate of the vertical mantle melt flux is 0.005–0.1 m yr^{-1}. This figure is obtained by assuming that melt is produced by 5–10% partial melting, caused by

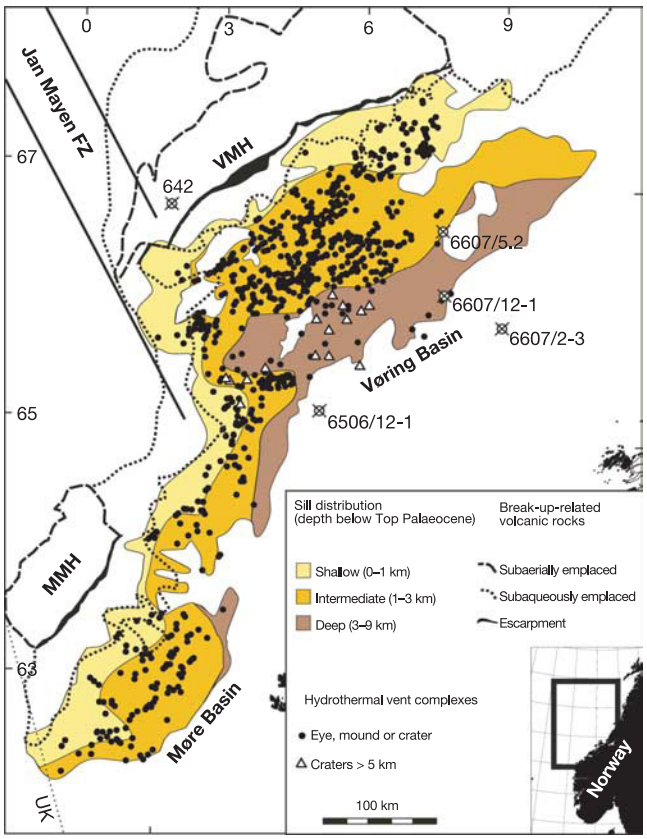

Figure 1 Distribution of hydrothermal vent complexes and volcanic intrusive and extrusive complexes on the mid-Norwegian continental margin. The map is based on detailed seismic mapping of >150,000 km of high-quality 2D seismic data and one 3D seismic survey (see Methods). Extrusive domains modified from ref. 31. The 'Inner Flows' is the subaqueous lavas emplaced landward of the escarpments. VMH, Vøring Marginal High; MMH, Møre Marginal High; FZ, fracture zone.

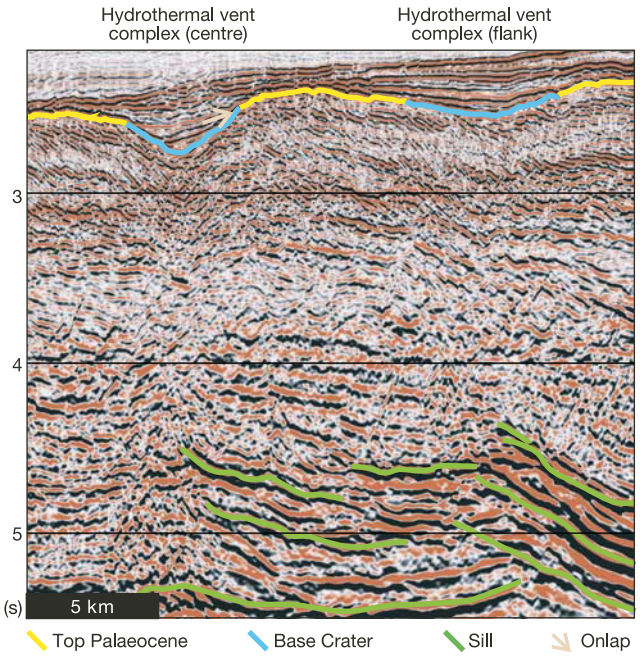

Figure 2 Seismic example of hydrothermal vent complexes in the southeast Vøring Basin. Two ~5 km-wide explosion craters are located at the Top Palaeocene level. The craters document the explosive power of the phreatic eruptions forming the hydrothermal vent complexes. Note the erosional base of the craters, onlapping sedimentary strata, disrupted chimney zones surrounded by inward-dipping strata below the craters, and a deep sill complex terminating below the craters. The craters are fairly rare (9%). The upper part of most hydrothermal vent complexes are eye-shaped (61%) or dome-shaped (30%), and less than 2 km in diameter (62%). Most hydrothermal vent complexes originate above the termination of a transgressive sill reflection, as shown by this example. Time shown in seconds (s) is the two-way travel-time for the seismic pulse.

decompression of mantle, that rises at a velocity of 0.1–1 m yr^{-1} (ref. 19). The calculated flux range is consistent with the flux obtained from observational data in the NAVP[20] (average melt flux of 0.0064 m yr^{-1}, assuming that two-thirds of the melt volume was emplaced in 500,000 yr). The flux rates show that it will take 1,000–60,000 yr to produce the observed 100–300-m-thick sills complex without any focusing of mantle-derived melts.

The sills in the Møre and Vøring basins were mainly intruded into organic-rich Cretaceous and Palaeocene mudstones[7,10]. The organic carbon is partly converted into methane when sedimentary rocks are heated beyond the gas window (~100–200 °C; ref. 21). Accordingly, the methane production potential of an intruded sedimentary basin can be estimated from the total organic carbon (TOC) content of the sedimentary sequences and the volume and thermal history of the rocks heated by the intruding sills. We define a 'contact metamorphic aureole' as the volume of rocks heated beyond 100 °C following the sill emplacement. As a rule of thumb, the thickness of the metamorphic aureole is comparable to, or greater, than the sill thickness on both sides of thick (>50 m) sills intruded into shales[6,22,23]. The thermogenic methane produced from organic material in contact aureoles has a depleted carbon isotope ratio ($\delta^{13}C = -35$ to -50‰)[21].

From Fig. 4 we estimate that 0.3 to 3.0×10^{18} g of methane was produced in the metamorphic aureoles in the Vøring and Møre basins just after the sill emplacement. The methane production in the entire NAVP is possibly five times higher. It has been estimated that a release of 1.1×10^{18} g of CH_4 ($\delta^{13}C = -60$‰) is sufficient to cause the >2.5‰ negative excursion in carbon isotopes during the IETM[3]. Mass-balance calculations show that rapid release of the thermogenic methane produced in the metamorphic aureoles in the Vøring and Møre basins ($0.3–3.0 \times 10^{18}$ g CH_4) results in a carbon isotope excursion of -0.2 to -3.0‰ in the (present-day) exchangeable carbon reservoir (see ref. 3). Correspondingly, the minimum excursion resulting from methane release in the entire NAVP is -1.0‰.

Recent work indicates that surface temperatures across all latitudes rose by 6 to 8 °C during the IETM, implying a rapid and massive release of carbon to the atmosphere[24]. Extrusive volcanism accompanying and following the intrusive activity may have led to the release of vast amounts of greenhouse gases and aerosols in the NAVP (about 10^{20} g CO_2)[25]. However, the extrusive phase took place over a 2–3-Myr period, leading to average fluxes of only 10^{13} g CO_2 yr^{-1}. Melt intruded into organic-rich sedimentary basins may cause considerably higher carbon fluxes into the atmosphere than a similar volume of erupted magma. Degassing of one cubic metre of CO_2-saturated basaltic melt may release about 3.6 kg of carbon[26], whereas a melt intruded into organic-rich mudstones may trigger the release of 25–100 kg of carbon per cubic metre of magma. Hence, the carbon flux into the atmosphere would easily be more than an order of magnitude higher if the melt intruded into a relatively organic-rich sedimentary sequence rather than being erupted and degassed at the surface.

Contact metamorphism of organic material and associated methane venting in NAVP has the potential to cause the IETM $\delta^{13}C$ excursion if the methane is transported to the ocean or atmosphere. Our data suggest that the observed hydrothermal vent complexes represent efficient pathways for vertical fluid transport in sedimentary basins. In addition, gas from accumulations higher in the stratigraphy could be released when pierced by the

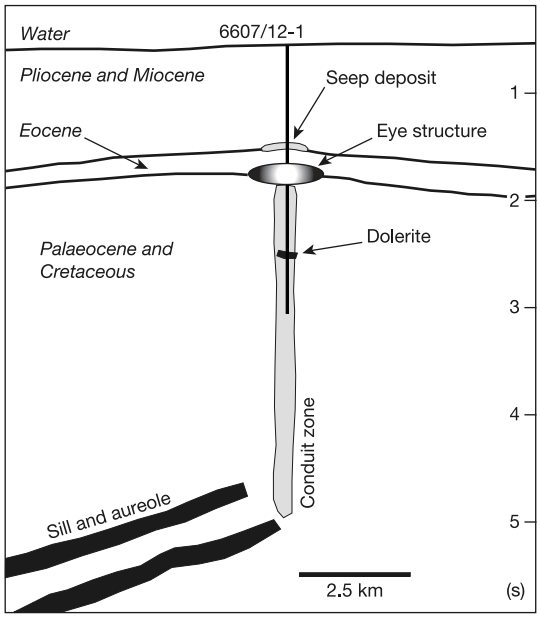

Figure 3 Schematic line drawing of a seismic profile across the hydrothermal vent complex drilled by 6607/12-1. A vertical zone of disturbed seismic data is interpreted as a conduit zone connecting the tip of a sill intrusion with the palaeo-surface. The eye-shaped structure represents the upper part of the complex, probably formed by filling of an explosion crater. Similar relationships between sills, conduit zone and palaeo-surface deposits are observed in most of the >700 hydrothermal vent complexes identified in the Vøring and Møre basins. Seep deposits above the eye shows that the vent complexes may be re-used for fluid migration a long time after their formation.

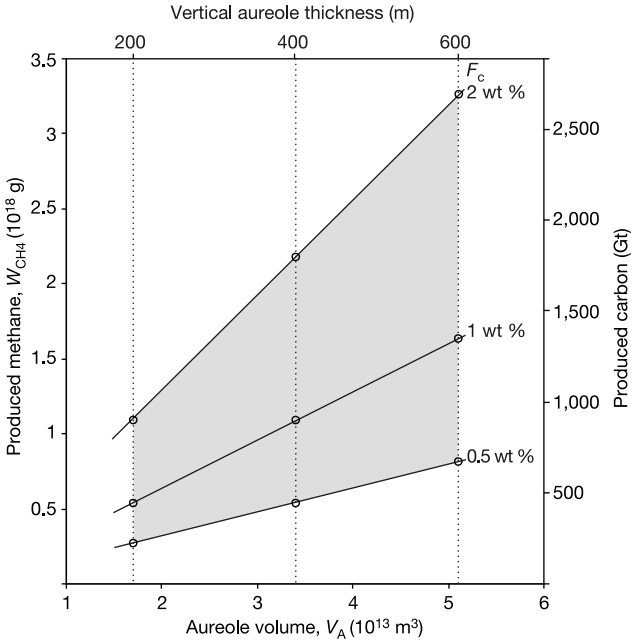

Figure 4 Estimated methane production potential of the Vøring and Møre basins. This is plotted as a function of the volume of the metamorphic aureole, V_A, and the amount of carbon transferred to methane, F_C. The mass of methane, W_{CH4}, produced in a contact metamorphic aureole is:

$$W_{CH4} = 1.34 F_C V_A \rho$$

where 1.34 is the atomic weight conversion factor between carbon and methane, and ρ is the rock density ($\rho = 2{,}400$ kg m^{-3}). The range of V_A is based on the mapped extent of the sill complex (85,000 km^2) and an average integrated vertical aureole thickness of 200 to 600 m. A realistic range of F_C is 0.5 to 2.0 wt % (see Methods). An estimate of the amount of gas ultimately produced from the original organic carbon during maturation and metamorphism is 50–90%, depending on the kerogen type[21]. Finally, note that we have not included the possible contribution from sediment decarbonation reactions, magma degassing, or shallow gas reservoirs pierced by the hydrothermal vent complexes.

hydrothermal vent complexes. Methane erupted beneath the sea from the hydrothermal vent complexes will probably reach the atmosphere. This is supported by numerical modelling showing that rising methane plumes formed by subaqueous gas eruptions provide efficient means of transporting methane through the water column without being dissolved or oxidized[27].

The seismic and biostratigraphic data strongly suggest a temporal correlation between the sill emplacement and the IETM, but the data do not have the ~10,000-yr resolution required to firmly establish this link. However, this could be proved by coring the Palaeocene–Eocene boundary strata on the flanks of one or more hydrothermal vent complexes, and identifying the negative carbon isotope excursion and its relation to deposits from the vent complexes.

We conclude that explosive release of metamorphic thermogenic methane during the intrusive phase of NAVP may have caused the extraordinary warming during the IETM. For reference, the average anthropogenic release of carbon during the 1990s was 6.3×10^{15} g carbon per year (ref. 28), which corresponds to a release of all the produced metamorphic CH_4 in the Vøring and Møre basins during a period of 35–360 yr.

Our observations stress the link between large igneous provinces (LIPs) and global climate changes. The climate impact of a LIP may be considerable if the melt is partly or completely emplaced into carbon-rich sedimentary successions. Volcanic basins thus provide a setting for rapid perturbations of the otherwise steady release of carbon from the sedimentary reservoirs. Several other major LIPs temporally correlated with prominent negative carbon isotope anomalies contain extensive subvolcanic intrusive complexes in carbon-rich sedimentary sequences, including the Siberian Traps (~250 Myr ago; the Permo-Triassic boundary), and the Karoo Igneous Province (~183 Myr ago; the Early–Middle Jurassic boundary) (compare with ref. 29). □

Methods

The seismic interpretation was done on a comprehensive seismic database consisting of more than 150,000 km of high-quality industrial multichannel seismic data and one 2,000 km^3 3D seismic survey using the Kingdom Suite seismic interpretation software. High-pass-filtered Bouguer gravity data and high-resolution aeromagnetic data were also loaded in the workstation project, and used to constrain the seismic interpretation.

The sill complex was carefully interpreted on the basis of seismic characteristics, in particular high reflection amplitude, saucer shape, local transgressive segments, and abrupt reflection termination. The interpretation was corroborated by analysis of potential field data and local pre-stack analysis of the seismic data, including re-processing and modelling. The sill complex interpretation was tied to well 6607/5-2, which penetrated three sill intrusions.

The hydrothermal vent complexes were similarly interpreted using seismic characteristics. The vent complexes are characterized by a circular eye-shaped, dome-shaped or crater-shaped upper part and a chimney-like lower part with disturbed seismic character commonly surrounded by inward-dipping reflections and bright reflections[11–13]. Seismic evidence of fluid migration is commonly located in sedimentary strata above the vent complexes, such as chimneys, mounds, bright spots and flat spots. The disturbances sometimes continue all the way to the present sea floor. The location, size and seismic characteristics of each interpreted hydrothermal vent complex have been carefully described and stored in an electronic database. The seismic interpretation and mapping has been conducted in parallel with fieldwork on the intrusive and hydrothermal vent complexes in the Karoo Basin and numerical modelling studies of formation of hydrothermal vent complexes[11].

The well 6607/12-1 was drilled 2 km into the centre of a hydrothermal vent complex in 1986, and provides a unique opportunity to describe and analyse the properties of a vent complex. We have completed a comprehensive study of the seismic data, wireline log data, and core data and cuttings from this well. Samples (139 in total) were collected and analysed by scanning electron microscope and microprobe, X-ray diffraction (104 samples), isotope analysis (carbon, oxygen and strontium; 76 analyses), organic geochemistry (RockEval and total organic carbon; 67 samples), and vitrinite reflectance (78 samples). In addition, the biostratigraphy of the well was re-analysed, with particular focus on accurate dating of the Palaeocene and Eocene sequences. The data are partly described in ref. 12. Vitrinite reflectance data strongly suggest that the conduit zone of the hydrothermal vent complex is affected by hydrothermal fluids. The conduit zone is characterized by vitrinite reflectance values of up to 4.3%R_o, where %R_o is the vitrinite reflectance, compared with background values in the range 0.2–0.3%R_o.

Limited data on total organic carbon (TOC) values and kerogen type are published in the Vøring and Møre basins. TOC values in Upper Cretaceous sediments in wells 6607/2-3 and 6506/12-5 (Fig. 1) range from 0.4 to 2.6 wt % (mean = 1.4; standard deviation = 0.44; $N = 53$)[30], but was probably higher during the Palaeocene. Shales with source-rock quality may also be present within the intruded sequences[10].

Received 1 September 2003; accepted 4 April 2004; doi:10.1038/nature02566.

1. Kennett, J. P. & Stott, L. D. Abrupt deep-sea warming, palaeoceanographic changes and benthic extinctions at the end of the Palaeocene. *Nature* **353,** 225–229 (1991).
2. Schmitz, B. & Pujalte, V. Sea-level, humidity, and land-erosion records across the initial Eocene thermal maximum from a continental-marine transect in northern Spain. *Geology* **31,** 689–692 (2003).
3. Dickens, G. R., O'Neil, J. R., Rea, D. K. & Owen, R. M. Dissociation of oceanic methane hydrate as a cause of the carbon isotope excursion at the end of the Paleocene. *Paleoceanography* **10,** 965–971 (1995).
4. Dickens, G. R., Castillo, M. M. & Walker, J. C. G. A blast from the latest Paleocene: simulating first-order effects of massive dissociation of oceanic methane hydrate. *Geology* **25,** 259–262 (1997).
5. Skogseid, J., Pedersen, T., Eldholm, O. & Larsen, B. T. Tectonism and magmatism during NE Atlantic continental break-up: the Vøring Margin. *Geol. Soc. Spec. Publ.* **68,** 305–320 (1992).
6. Berndt, C., Skogly, O. P., Planke, S. & Eldholm, O. High-velocity breakup-related sills in the Vøring Basin, off Norway. *J. Geophys. Res.* **105,** 28443–28454 (2000).
7. Brekke, H. The tectonic evolution of the Norwegian Sea Continental Margin with emphasis on the Vøring and Møre Basins. *Geol. Soc. Spec. Publ.* **167,** 327–378 (2000).
8. Smallwood, J. R. & Maresh, J. The properties, morphology and distribution of igneous sills: modelling, borehole data and 3D seismic from the Faroe-Shetland area. *Geol. Soc. Spec. Publ.* **197,** 271–306 (2002).
9. Chevallier, L. & Woodford, A. C. Morpho-tectonics and mechanism of emplacement of the dolerite rings and sills of the western Karoo, South Africa. *S. Afr. J. Geol.* **102,** 43–54 (1999).
10. Brekke, H., Dahlgren, S., Nyland, B. & Magnus, C. The prospectivity of the Vøring and Møre basins on the Norwegian Sea continental margin. in *Petrol. Geol. NW Eur. Proc. 5th Conf.* (eds Fleet, A. J. & Boldy, S. A. R.) 261–274 (Geol. Soc. Publ., London, 1999).
11. Jamveit, B., Svensen, H., Podladchikov, Y. & Planke, S. Hydrothermal vent complexes associated with sill intrusions in sedimentary basins. *Geol. Soc. Lond. Spec. Publ.*(in the press).
12. Svensen, H., Jamtveit, B. & Planke, S. Seep carbonate formation controlled by hydrothermal vent complexes: a case study from the Vøring volcanic basin, the Norwegian Sea. *Geo-Mar. Lett.* **23,** 351–358 (2003).
13. Planke, S., Rasmussen, T., Rey, S. S. & Myklebust, R. Seismic characteristics and distribution of volcanic intrusions and hydrothermal vent complexes in the Vøring and Møre basins. In *Petrol. Geol. NW Europe and Global Perspectives—Proc. 6th Petrol. Geol. Conf.* (eds Tony Dore, T. & Vining, B.) (Geol. Soc. Publ., London, in the press).
14. Woodford, A. C., *et al. Hydrogeology of the Main Karoo Basin: Current Knowledge and Research Needs* (Water Research Commission report 860, WRC, Pretoria, 2001).
15. Berggren, W. A., Kent, D. V., Swisher, C. C. & Aubry, M.-P. A revised Cenozoic geochronology and chronostratigraphy. *Soc. Sed. Geol. Spec. Publ.* **54,** 129–212 (1995).
16. Crouch, E. M. *et al.* Global dinoflagellate event associated with the late Paleocene thermal maximum. *Geology* **29,** 315–318 (2001).
17. Trude, J., Cartwright, J., Davies, R. J. & Smallwood, J. New technique for dating igneous sills. *Geology* **31,** 813–816 (2003).
18. Hopper, P. R. The Columbia River flood basalt province: Current Status. *AGU Geophys. Monogr.* **100,** 1–28 (1997).
19. Weinberg, R. F. & Podladchikov, Y. Diapiric ascent of magmas through power-law crust and mantle. *J. Geophys. Res.* **99,** 9543–9559 (1994).
20. Eldholm, O. & Grue, K. North Atlantic volcanic margins: dimensions and production rates. *J. Geophys. Res.* **99,** 2955–2968 (1995).
21. Hunt, J. M. *Petroleum Geochemistry and Geology* (W. H. Freeman, San Francisco, 1996).
22. Kjeldstad, A., Langtangen, H. P., Skogseid, J. & Bjørlykke, K. in *Advanced Topics in Computation Partial Differential Equations—Numerical Methods and Diffpack Programming* (eds Langtangen, H. P. & Tveito, A.) 611–656 (Springer, 2003).
23. Galushkin, Y. I. Thermal effects of igneous intrusions on maturity of organic matter: a possible mechanism of intrusion. *Org. Geochem.* **26,** 645–658 (1997).
24. Zachos, J. C. *et al.* A transient rise in tropical sea surface temperature during the Paleocene-Eocene thermal maximum. *Science* **302,** 1551–1554 (2003).
25. Eldholm, O. & Thomas, E. Environmental impact of volcanic margin formation. *Earth Planet. Sci. Lett.* **117,** 319–329 (1993).
26. Caldeira, K. & Rampino, M. R. The mid-Cretaceous super plume, carbon dioxide, and global warming. *Geophys. Res. Lett.* **18,** 987–990 (1991).
27. Zhang, Y. Methane escape from gas hydrate systems in marine environment, and methane-driven oceanic eruptions. *Geophys. Res. Lett.* **30,** doi:10.1029/2002GL016658 (2003).
28. IPCC (Intergovernmental Panel on Climate Change). *Climate Change 2001: The Scientific Basis* (IPCC, Geneva, 2001).
29. Wignall, P. B. Large igneous provinces and mass extinctions. *Earth Sci. Rev.* **53,** 1–33 (2001).
30. Eckhoff, E. E. *Foraminiferstratigrafi og Faunautvikling i Turbidittfacies fra Over Kritt på Midtnorsk Sokkel* Candidatus Scientiarum thesis, Dept Geol., Univ. Oslo (1999).
31. Berndt, C., Planke, S., Alvestad, E., Tsikalas, F. & Rasmussen, R. Seismic volcanostratigraphy of the Norwegian Margin: constraints on tectonomagmatic break-up processes. *J. Geol. Soc. Lond.* **158,** 413–426 (2001).

Acknowledgements This study was supported by grants (H.S. and B.J.) from the Norwegian Research Council. We thank TGS-NOPEC for access to seismic data, H. Selnes for the biostratigraphic dating, and G. R. Dickens and J. G. Feder for comments on the manuscript.

Competing interests statement The authors declare that they have no competing financial interests.

Correspondence and requests for materials should be addressed to H.S. (hsvensen@geo.uio.no) or S.P. (planke@vbpr.no).